Supporting Information for "Barchan dunes cruising dune-size obstacles"

W. R. Assis[1], D. S. Borges[1], E. M. Franklin[1]

[1]School of Mechanical Engineering, UNICAMP – University of Campinas,

Rua Mendeleyev, 200, Campinas, SP, Brazil

Contents of this file

Additional Supporting Information (Files uploaded separately)

1. Captions for Movies S1 to S8

Introduction

This supporting information presents the layout of the experimental device, microscopy images of the used grains, images of the used obstacles, snapshots of barchans of different grain types interacting with different obstacles, and movies showing examples of barchan–obstacle interaction. All movies have been sped up by 30x. We note that individual images and movies used in the manuscript are available on Mendeley Data (http://dx.doi.org/10.17632/snffc3wvfp.1).

The experiments described in the paper were conducted in the experimental setup shown in Figure S1. It consisted basically of a water reservoir, two centrifugal pumps, a flow straightener, a 5-m-long closed-conduit channel, a settling tank, and a return line. The channel was transparent, and we placed the desired obstacle in the test section prior to each experiment. The obstacles used in this work are depicted in Figure S7. Also, prior to each experiment, and with the channel already filled with water, we poured the desired quantity of particles in the test section, forming a conical heap of known mass and composition. The tests begin by imposing the water flow, and then filming the interaction between the resulting barchan and the obstacle. The test conditions are listed in Figure S16.

For recording the images, we used a camera of complementary metal-oxide-semiconductor (CMOS) type placed above the channel, so that it acquired top view images of the bedform while it interacted with the obstacle. The camera resolution was of 1920 px $\times$ 1080 px at 60 Hz, and it was mounted on a traveling system. Depending on the test run, the region of interest (ROI) was set to either 1636 px $\times$ 926 px, 1761 px $\times$ 926 px or 1806 px $\times$ 926 px, and the frequency to 60 Hz. We used a lens of 18 – 105 mm focal distance mounted on the camera, and lamps of light-emitting diode (LED) branched to a continuous-current source for lighting. The conversion from px to a physical system of units was computed from images of a scale (placed in the channel filled with water). The acquired images were afterward processed by numerical scripts. Examples of images showing the barchan-obstacle interactions are shown in Figures S8 and S9.

We made use of the machine learning method Support Vector Machine (SVM) for organizing our data and proposing the maps shown in Figure 3 in the paper. SVM is a supervised method that can be used for classification. Given a cloud of data and assuming that they are linearly separable, SVM searches for a hyperplane that maximizes the separation between two classes, thus performing binary classification. It is possible to adapt SVM to handle situations where the points in the cloud are not linearly separable. The *Cover's Theorem* states that data that are not linearly separable can be turned into it by projecting them into a higher-dimensional space through a nonlinear transformation (Cover, 1965). When the decision boundary in this higher-dimensional space is projected back into the original space, it appears as a curved decision boundary (p.149, Rhys, 2020). SVM can be further extended to solve multiclass problems by dividing them into multiple binary classification problems (usually using heuristic methods, Kowalczyk, 2017). In the present work, two methods were used, the *one-versus-all* and the *one-versus-one*, both of which yielded similar results. We also made use of *Scikit-learn* (Pedregosa et al., 2011), an open-source Python library that implements a variety of machine learning algorithms and visualization tools.

References

Cover, T. M. (1965). Geometrical and statistical properties of systems of linear inequalities with applications in pattern recognition. *IEEE Transactions on Electronic Computers*, *EC-14*(3), 326-334. doi: 10.1109/PGEC.1965.264137

Kowalczyk, A. (2017). *Support vector machines succinctly.* Syncfusion Inc.

Pedregosa, F., Varoquaux, G., Gramfort, A., Michel, V., Thirion, B., Grisel, O., ...

Duchesnay, E. (2011). Scikit-learn: Machine learning in Python. *Journal of Machine Learning Research*, *12*, 2825–2830. Retrieved from http://jmlr.org/papers/v12/pedregosa11a.html

Rhys, H. (2020). *Machine learning with R, the tidyverse, and mlr*. Manning Publications.

Movie S1. 1a.avi Movie showing top views of the evolution of a barchan interacting with a cylinder (pass over case, corresponding to the snapshots of Fig. 1a of the paper). The video is sped up by 30x.

Movie S2. 1b.avi Movie showing top views of the evolution of a barchan interacting with a cylinder (transient case, corresponding to the snapshots of Fig. 1b of the paper). The video is sped up by 30x.

Movie S3. 1c.avi Movie showing top views of the evolution of a barchan interacting with a cylinder (bypass case, corresponding to the snapshots of Fig. 1c of the paper). The video is sped up by 30x.

Movie S4. 1d.avi Movie showing top views of the evolution of a barchan interacting with a cylinder (pass over case, corresponding to the snapshots of Fig. 1d of the paper). The video is sped up by 30x.

Movie S5. 2a.avi Movie showing top views of the evolution of a barchan interacting with a block (pass over case, corresponding to the snapshots of Fig. 2a of the paper). The video is sped up by 30x.

Movie S6. 2b.avi Movie showing top views of the evolution of a barchan interacting with a block (transient case, corresponding to the snapshots of Fig. 2b of the paper). The video is sped up by 30x.

Movie S7. 2c.avi Movie showing top views of the evolution of a barchan interacting with a sphere (bypass case, corresponding to the snapshots of Fig. 2c of the paper). The video is sped up by 30x.

Movie S8. 2d.avi Movie showing top views of the evolution of a barchan interacting with a block (trapping case, corresponding to the snapshots of Fig. 2d of the paper). The video is sped up by 30x.

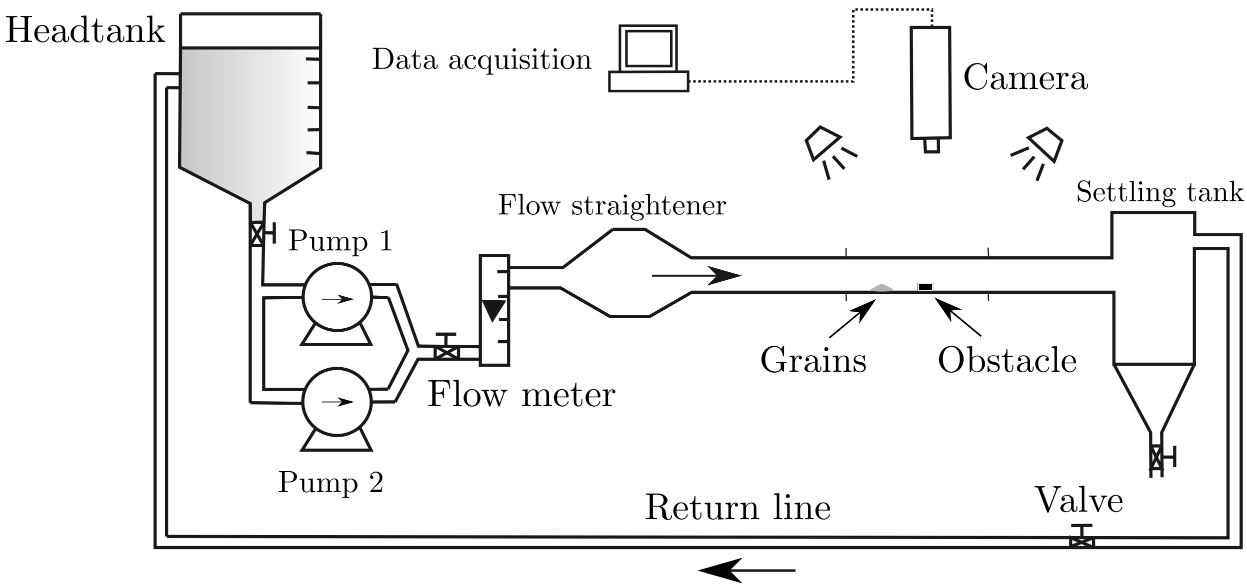

Figure S1. Layout of the experimental setup.

Figure S2. Photographs of some parts of the experimental setup. (a) View in perspective showing the water tank (blue cylinder on the top left), centrifugal pumps (below the tank), flow straightner and developing section (in acrylic on the right), and tent (blue structure on the right) where the test section is in. (b) Water tank. (c) Test section (inside the tent). (d) Settling tank.

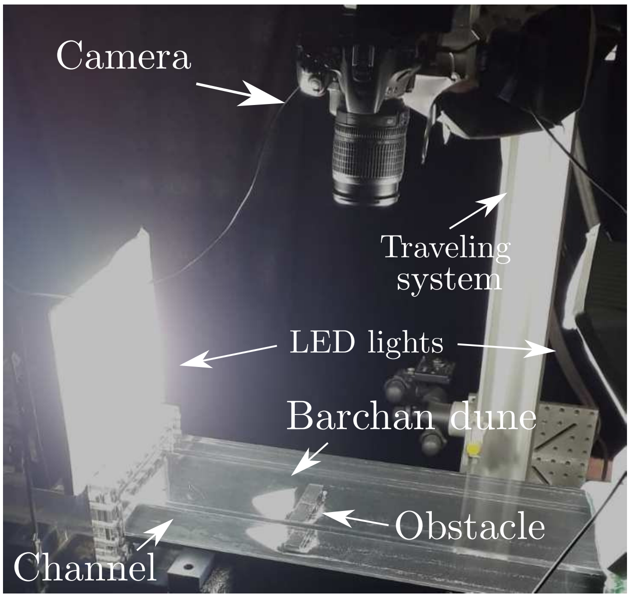

Figure S3. Photograph of the test section.

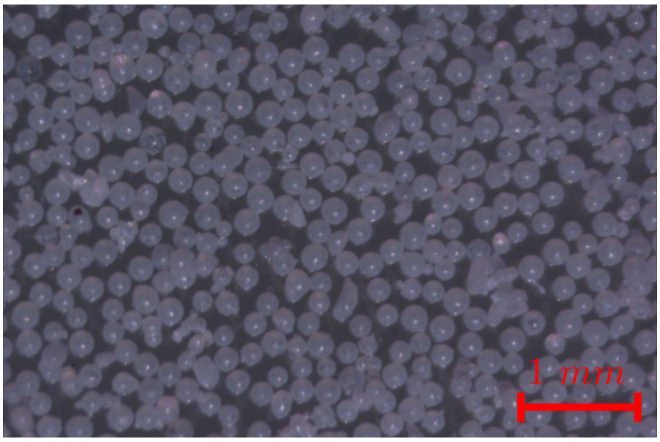

Figure S4. Microscopy image for the 0.15 mm $\leq d \leq$ 0.25 mm glass spheres.

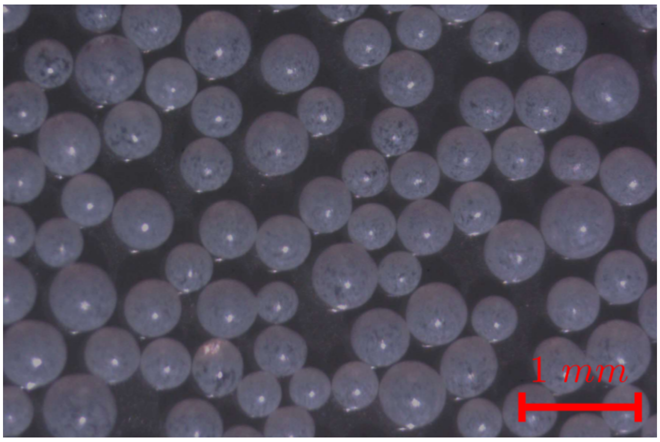

Figure S5. Microscopy image for the 0.40 mm $\leq d \leq$ 0.60 mm glass spheres.

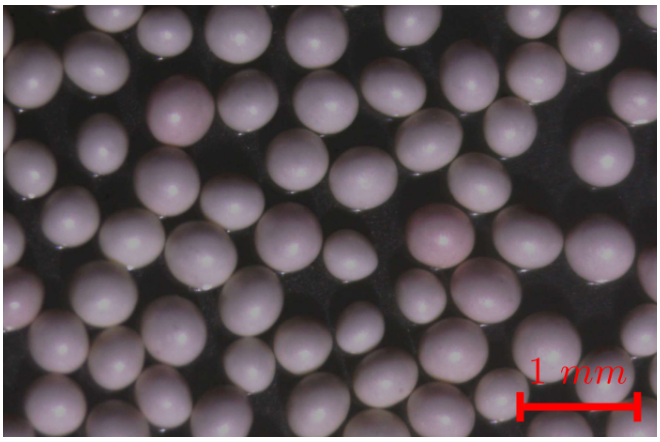

Figure S6. Microscopy image for the 0.40 mm $\leq d \leq$ 0.60 mm zirconium spheres.

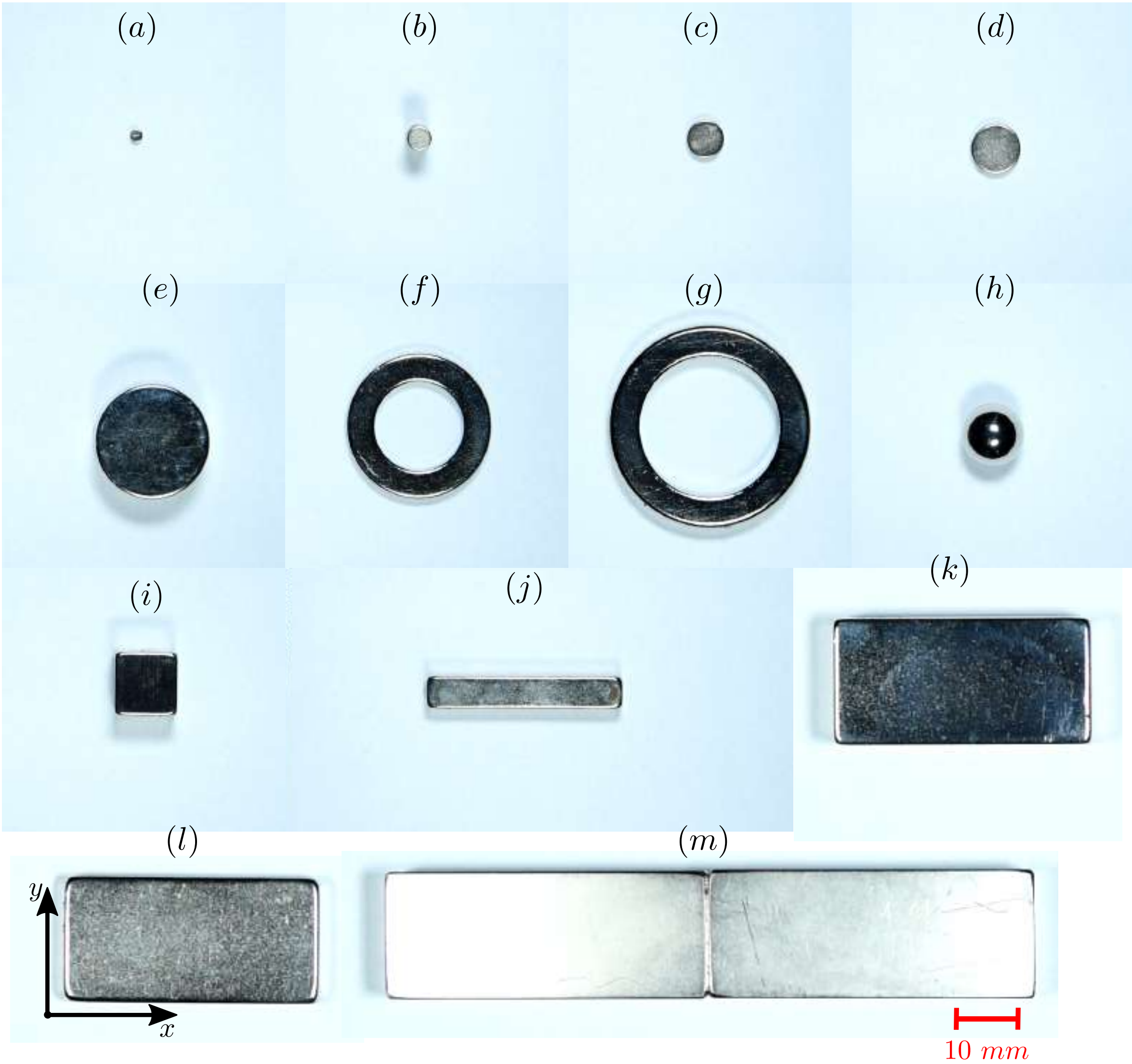

Figure S7. Top-view images of obstacles used in the tests. The dimensions of each object are listed in Table S1.

Table S1. Geometry and dimension of the obstacle depicted in each panel of Fig. S7.

Figure	Geometry	External diameter or length (mm)	Internal diameter or width (mm)	Height (mm)	Flow direction
S7(a)	cylinder	2.0	$\cdots$	1.5	x
S7(b)	cylinder	4.0	$\cdots$	2.0	x
S7(c)	cylinder	6.0	$\cdots$	2.0	x
S7(d)	cylinder	8.0	$\cdots$	2.0	x
S7(e)	cylinder	18.0	$\cdots$	10.0	x
S7(f)	ring	23	14	5	x
S7(g)	ring	32	22	5	x
S7(h)	sphere	10	$\cdots$	$\cdots$	x
S7(i)	block	10	10	10	x
S7(j)	block	30	5	5	x and y
S7(k)	block	40	18	5	x and y
S7(l)	block	40	20	10	x and y
S7(m)	block	100	20	10	y

(a) (b) (c) (d) (e)

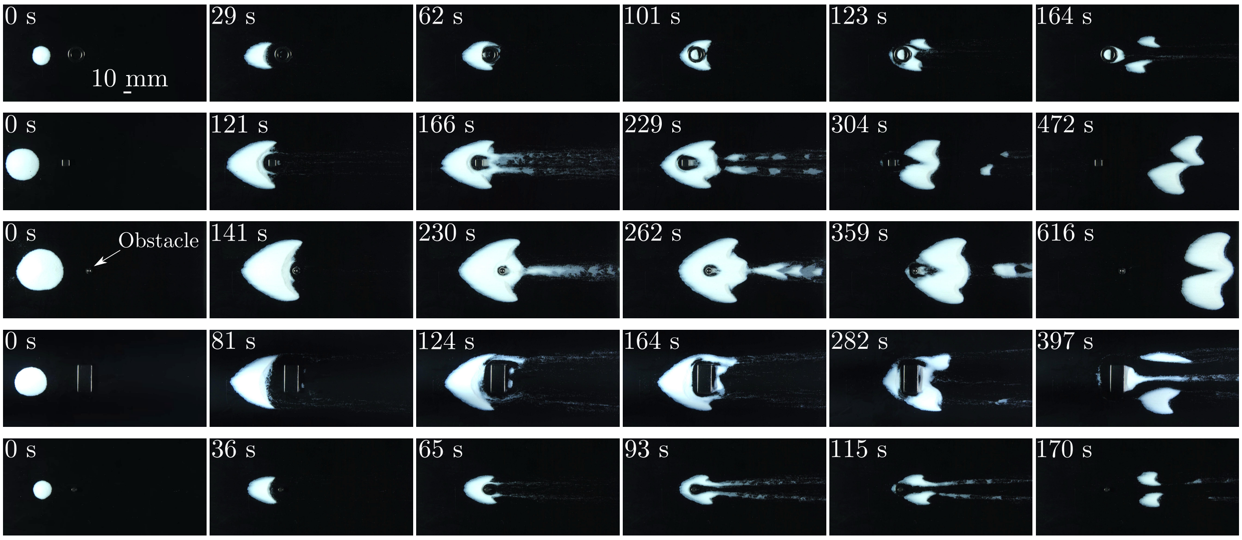

Figure S8. Snapshots of a barchan dune interacting with an obstacle, for different obstacle shapes. In the snapshots, the water flow is from left to right, and the corresponding times are shown in each frame. (a) A ring (test 58 in Figure S16), for which the dune shows a transient behavior; (b) a block (test 31 in Figure S16), for which the dune bypasses the obstacle; (c) a sphere (test 37 in Figure S16), for which the dune bypasses the obstacle; (d) a block (test 28 in Figure S16), for which the dune bypasses the obstacle; and (e) a cylinder (test 52 in Figure S16), for which the dune bypasses the obstacle. The obstacle appears as a bright metallic object in the images.

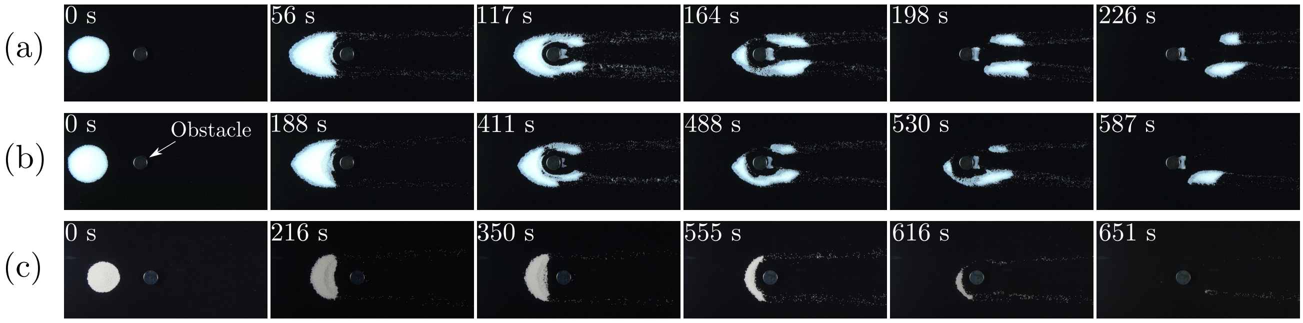

Figure S9. Snapshots of a barchan dune interacting with an obstacle of cylindrical shape, for different grain densities. In the snapshots, the water flow is from left to right, and the corresponding times are shown in each frame. (a) Glass spheres (test 26 in Figure S16), for which the dune bypasses the obstacle; (b) glass spheres (test 27 in Figure S16), for which the dune bypasses the obstacle; and (c) zirconium spheres (test 7 in Figure S16), for which the dune bypasses the obstacle. The obstacle appears as a bright metallic object in the images.

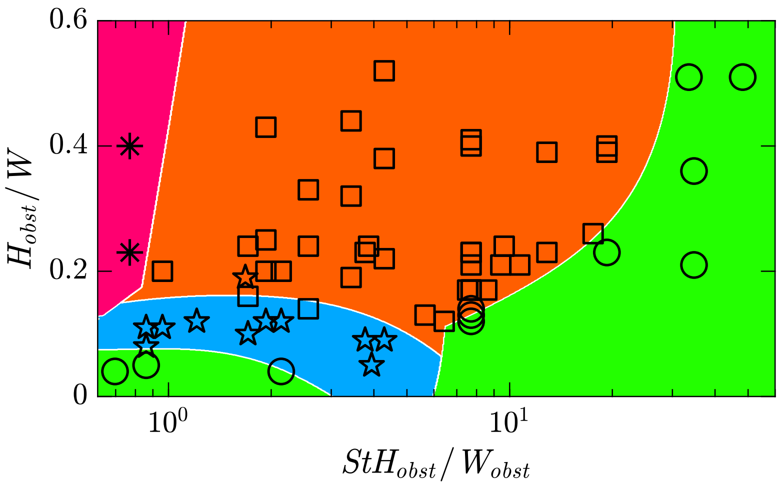

Figure S10. Map for the output of the barchan-obstacle interactions in the H_{obst}/W vs. StH_{obst}/W_{obst} space, drawn by machine learning (Support Vector Machine method). Squares, pentagrams, circles and asterisks correspond to bypass, transient, pass over and trapping patterns, respectively.

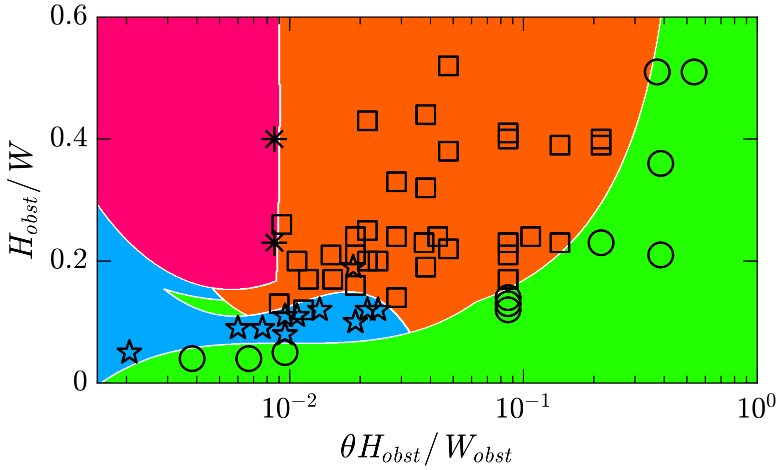

Figure S11. Map for the output of the barchan-obstacle interactions in the H_{obst}/W vs. $\theta H_{obst}/W_{obst}$ space, drawn by machine learning (Support Vector Machine method). Squares, pentagrams, circles and asterisks correspond to bypass, transient, pass over and trapping patterns, respectively.

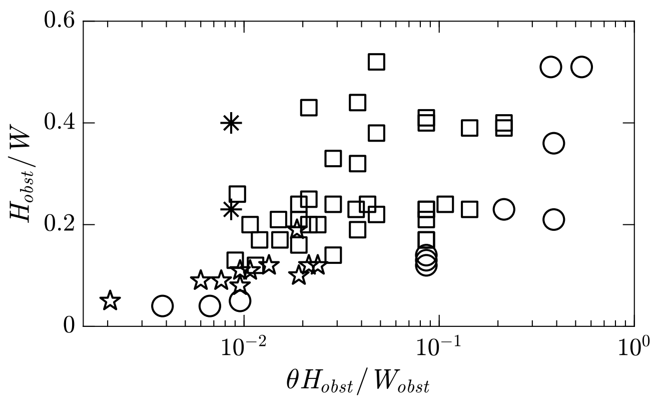

Figure S12. Different behaviors observed in the size ratio – modified Shields number space, i.e., H_{obst}/W vs. $\theta H_{obst}/W_{obst}$. Squares, pentagrams, circles and asterisks correspond to bypass, transient, pass over and trapping patterns, respectively.

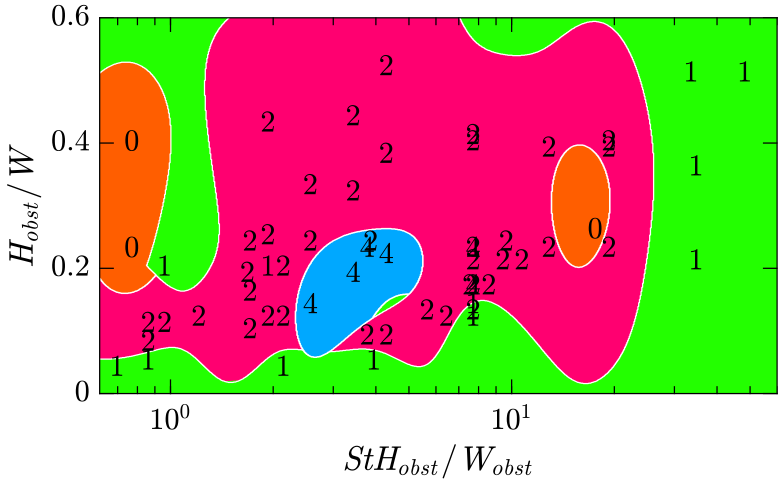

Figure S13. Number of resulting bedforms observed in the H_{obst}/W vs. StH_{obst}/W_{obst} diagram, drawn by machine learning (Support Vector Machine method).

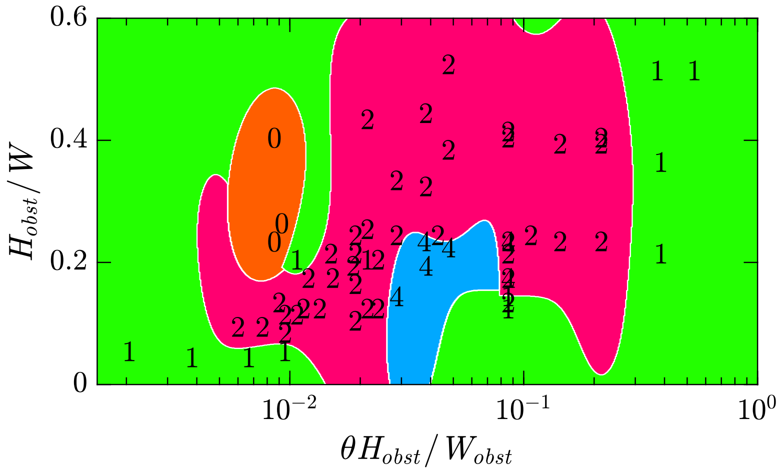

Figure S14. Number of resulting bedforms observed in the H_{obst}/W vs. $\theta H_{obst}/W_{obst}$ diagram, drawn by machine learning (Support Vector Machine method).

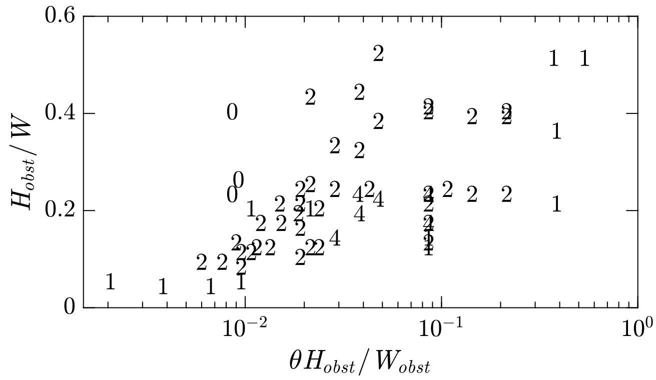

Figure S15. Number of resulting bedforms observed in the size ratio – modified Shields number space, i.e., H_{obst}/W vs. $\theta H_{obst}/W_{obst}$.

Test #	Obstacle	H_{obs}	W_{obs}	St	St (H_{obs}/W_{obs})	m	ρ_s/ρ	d	u_*	W	H_{obs}/W	Output
-	-	m	m	-	-	g	-	mm	m/s	m	-	-
1	Cylinder	0.01	0.018	7.7	4.29	8.0	2.5	0.2	0.0159	0.0464	0.22	bypass
2	Cylinder	0.01	0.018	7.7	4.29	1.5	2.5	0.2	0.0159	0.0264	0.38	bypass
3	Cylinder	0.01	0.018	7.7	4.29	0.5	2.5	0.2	0.0159	0.0193	0.52	bypass
4	Cylinder	0.01	0.018	6.8	3.77	8.0	2.5	0.2	0.0141	0.0435	0.23	bypass
5	Cylinder	0.01	0.018	19.3	10.71	8.0	2.5	0.5	0.0159	0.0468	0.21	bypass
6	Cylinder	0.01	0.018	17	9.42	8.0	2.5	0.5	0.0141	0.0486	0.21	bypass
7	Cylinder	0.01	0.018	31.6	17.57	8.0	4.1	0.5	0.0159	0.0384	0.26	bypass
8	Cylinder	0.002	0.018	7.7	0.86	8.0	2.5	0.2	0.0159	0.0423	0.05	pass over
9	Cylinder	0.002	0.018	7.7	0.86	1.5	2.5	0.2	0.0159	0.0241	0.08	transient
10	Cylinder	0.002	0.018	7.7	0.86	0.5	2.5	0.2	0.0159	0.0175	0.11	transient
11	Cylinder	0.002	0.018	19.3	2.14	8.0	2.5	0.5	0.0159	0.0472	0.04	pass over
12	Cylinder	0.002	0.018	35.5	3.94	8.0	4.1	0.5	0.0168	0.0384	0.05	transient
13	Cylinder	0.004	0.018	7.7	1.71	8.0	2.5	0.2	0.0159	0.0409	0.10	transient
14	Cylinder	0.004	0.018	7.7	1.71	1.5	2.5	0.2	0.0159	0.0245	0.16	bypass
15	Cylinder	0.004	0.018	7.7	1.71	0.5	2.5	0.2	0.0159	0.0170	0.24	bypass
16	Cylinder	0.004	0.018	19.3	4.29	8.0	2.5	0.5	0.0159	0.0467	0.09	transient
17	Cylinder	0.004	0.018	17	3.77	8.0	2.5	0.5	0.0141	0.0461	0.09	transient
18	Cylinder	0.006	0.018	7.7	2.57	8.0	2.5	0.2	0.0159	0.0426	0.14	bypass
19	Cylinder	0.006	0.018	7.7	2.57	1.5	2.5	0.2	0.0159	0.0247	0.24	bypass
20	Cylinder	0.006	0.018	7.7	2.57	0.5	2.5	0.2	0.0159	0.0182	0.33	bypass
21	Cylinder	0.006	0.018	19.3	6.43	8.0	2.5	0.5	0.0159	0.0483	0.12	bypass
22	Cylinder	0.006	0.018	17	5.65	8.0	2.5	0.5	0.0141	0.0471	0.13	bypass
23	Cylinder	0.008	0.018	7.7	3.43	8.0	2.5	0.2	0.0159	0.0429	0.19	bypass
24	Cylinder	0.008	0.018	7.7	3.43	1.5	2.5	0.2	0.0159	0.0249	0.32	bypass
25	Cylinder	0.008	0.018	7.7	3.43	0.5	2.5	0.2	0.0159	0.0181	0.44	bypass
26	Cylinder	0.008	0.018	19.3	8.57	8.0	2.5	0.5	0.0159	0.0468	0.17	bypass
27	Cylinder	0.008	0.018	17	7.53	8.0	2.5	0.5	0.0141	0.0480	0.17	bypass
28	Block	0.01	0.04	7.7	1.93	8.0	2.5	0.2	0.0159	0.0399	0.25	bypass
29	Block	0.01	0.04	7.7	1.93	1.5	2.5	0.2	0.0159	0.0232	0.43	bypass
30	Block	0.01	0.02	7.7	3.86	8.0	2.5	0.2	0.0159	0.0413	0.24	bypass
31	Block	0.01	0.01	7.7	7.71	8.0	2.5	0.2	0.0159	0.0440	0.23	bypass
32	Block	0.01	0.01	7.7	7.71	1.5	2.5	0.2	0.0159	0.0248	0.40	bypass
33	Sphere	0.01	0.01	7.7	7.71	8.0	2.5	0.2	0.0159	0.0430	0.23	bypass
34	Sphere	0.01	0.01	7.7	7.71	1.5	2.5	0.2	0.0159	0.0245	0.41	bypass
35	Block	0.01	0.01	7.7	7.71	20.0	2.5	0.2	0.0159	0.0588	0.17	bypass
36	Block	0.01	0.01	7.7	7.71	40.0	2.5	0.2	0.0159	0.0734	0.14	pass over
37	Sphere	0.01	0.01	7.7	7.71	20.0	2.5	0.2	0.0159	0.0574	0.17	bypass
38	Sphere	0.01	0.01	7.7	7.71	40.0	2.5	0.2	0.0159	0.0753	0.13	pass over
39	Block	0.005	0.02	7.7	1.93	8.0	2.5	0.2	0.0159	0.0426	0.12	transient
40	Block	0.005	0.02	7.7	1.93	1.5	2.5	0.2	0.0159	0.0253	0.20	bypass
41	Block	0.005	0.005	7.7	7.71	8.0	2.5	0.2	0.0159	0.0420	0.12	pass over
42	Block	0.005	0.005	7.7	7.71	1.5	2.5	0.2	0.0159	0.0243	0.21	bypass
43	Block	0.005	0.04	7.7	0.96	8.0	2.5	0.2	0.0159	0.0438	0.11	transient
44	Block	0.005	0.04	7.7	0.96	1.5	2.5	0.2	0.0159	0.0252	0.20	bypass
45	Block	0.005	0.018	7.7	2.14	8.0	2.5	0.2	0.0159	0.0433	0.12	transient
46	Block	0.005	0.018	7.7	2.14	1.5	2.5	0.2	0.0159	0.0248	0.20	bypass
47	Cylinder	0.009	0.002	7.7	34.71	8.0	2.5	0.2	0.0159	0.0426	0.21	pass over
48	Cylinder	0.009	0.002	7.7	34.71	1.5	2.5	0.2	0.0159	0.0253	0.36	pass over
49	Cylinder	0.01	0.004	7.7	19.28	8.0	2.5	0.2	0.0159	0.0431	0.23	pass over
50	Cylinder	0.01	0.004	7.7	19.28	1.5	2.5	0.2	0.0159	0.0248	0.40	bypass
51	Cylinder	0.01	0.006	7.7	12.86	8.0	2.5	0.2	0.0159	0.0433	0.23	bypass
52	Cylinder	0.01	0.006	7.7	12.86	1.5	2.5	0.2	0.0159	0.0257	0.39	bypass
53	Cylinder	0.01	0.008	7.7	9.64	8.0	2.5	0.2	0.0159	0.0422	0.24	bypass
54	Cylinder	0.01	0.004	7.7	19.28	1.5	2.5	0.2	0.0159	0.0257	0.39	bypass
55	Block	0.01	0.1	7.7	0.77	1.5	2.5	0.2	0.0159	0.0250	0.40	trapping
56	Block	0.01	0.1	7.7	0.77	8.0	2.5	0.2	0.0159	0.0431	0.23	trapping
57	Ring	0.005	0.032	7.7	1.21	8.0	2.5	0.2	0.0159	0.0431	0.12	transient
58	Ring	0.005	0.023	7.7	1.68	1.5	2.5	0.2	0.0159	0.0260	0.19	transient
59	Cylinder	0.002	0.018	6.27	0.70	8.0	2.5	0.2	0.0133	0.0477	0.04	pass over
60	Cylinder	0.01	0.0023	7.7	33.54	0.8	2.5	0.2	0.0159	0.0197	0.51	pass over
61	Cylinder	0.01	0.0016	7.7	48.21	0.8	2.5	0.2	0.0159	0.0194	0.51	pass over

Figure S16. List of tested conditions: obstacle geometry, obstacle height H_{obs}, obstacle width (frontal view) W_{obs}, Stokes number St, modified Stokes number StH_{obst}/W_{obst}, mass m, grain-water density ratio ρ_p/ρ, grain diameter d, friction velocity u_*, barchan width W, ratio between the obstacle height and dune width H_{obst}/W, and the output pattern.